

Ultra-High Optical Quality WS₂ Atomic-Layers via a Growth-Etch MOCVD Approach

Assael Cohen,[†] Avinash Patsha,[†] Pranab K. Mohapatra,[†] Miri Kazes,[‡] Lothar Houben,[§]
Dan Oron[‡] and Ariel Ismach^{†*}

[†]Department of Materials Science and Engineering, Tel Aviv University, Ramat Aviv, Tel Aviv, 6997801, Israel

[‡]Department of Physics of Complex Systems and [§]Department of Chemical Research Support, Weizmann Institute of Science, Rehovot 7610001, Israel

*aismach@tauex.tau.ac.il

Abstract

Metal organic chemical vapor deposition (MOCVD) is one of the main methodologies used for thin film fabrication in the semiconductor industry today and is considered one of the most promising routes to achieve large-scale and high-quality 2D transition metal dichalcogenides (TMDCs). However, MOCVD suffers from some serious drawbacks, such as small domain size (low crystallinity) and carbon contamination, resulting in poor optical quality, which may inhibit its implementation for the large-scale fabrication of atomic-thin semiconductors. Here we present a Growth-Etch MOCVD (GE-MOCVD) methodology, in which a small amount of water vapor is introduced during the growth, while the precursors are delivered in pulses. The evolution of the growth as a function of the amount of water vapor, the number and type of cycles and the gas composition is described. We show a domain size increase of more than four orders of magnitude relative to the conventional process. The improved crystal quality of WS₂ (and WSe₂) domains was demonstrated by means of Raman spectroscopy, photoluminescence (PL) spectroscopy and HRTEM studies. Moreover, time-resolved PL studies show a very long fluorescence lifetimes, comparable to those observed in mechanically exfoliated flakes. Thus, this unprecedented MOCVD-derived TMDC with ultra-high optical quality may open new opportunities to integrate such large-scale growth methodology into novel and existing technologies.

Introduction

2D materials offer many interesting properties to be used in novel existing technologies. One of the major bottle-necks in their successful integration in real-life applications is the need for reproducible large-scale growth of a high quality material. The pioneering work on the vapor-phase growth of single- and few-layer MoS₂¹ led to significant effort by the scientific community to realize methodologies for the large-area growth of 2D materials in general. As a result, extensive research has been carried to study chemical vapor deposition (CVD) growth of single- and few-layer atomic-films in general and transition metal dichalcogenides (TMDCs) in particular.¹⁻⁹ CVD of TMDCs often relies on the evaporation of metal oxide solid powders as the source for the transition metals (Mo, W, etc.) to be reacted with the chalcogen, usually obtained from a solid source as well. Despite the large volume of work and the great advance since then, metal-oxide based CVD growth has some significant drawbacks that inhibit its implementation for the study of the growth mechanism of such materials and for the consistent and rational growth of large-area 2D atomic-layers with the desired thickness and chemical composition. One of the main disadvantages is that the metal oxide precursors (MoO₃, WO₃, etc.) have relatively low vapor pressure, which forces their placement in proximity to the growth substrate *inside* the reactor chamber.^{1,6,10} This is an unwanted situation when depositing thin films using CVD,¹¹ as there is little control over the delivery of the metal precursor to the growth substrate. Furthermore, the metal oxide reacts with the chalcogen as well, thus causing undesirable and uncontrolled changes in the metal vapor flux during the growth.^{6,10} In addition, there is a strong effect of the position of the precursor on the growth, and thus, several different materials are often simultaneously grown within relatively small areas.^{6,10} Indeed, interesting attempts were developed in order to overcome these drawbacks, such as the re-oxidation of the sulfurized metal oxide precursor during growth or the asymmetric CVD system configuration¹² and the growth on a catalytic substrate.⁹ However, these partial solutions cannot lead to a consistent and well-controlled growth of single- and few-layer 2D materials to be used in large-scale applications. Moreover, the possibility to add dopants or alloying elements in a controlled manner, which is highly desirable for a wide range of applications, is very limited as well.

Indeed, learning from the vast thin film research in the past few decades, in particular from the chemical vapor deposition of Mo- and W-based thin films,^{13,14} volatile metal precursors were studied as well.^{3,15-19} In this scheme, metal-carbonyls and -halides are among the most promising precursors. Park *et. al.* pioneered the metal-organic CVD (MOCVD) of TMDCs using molybdenum- and tungsten-hexacarbonyl for the synthesis of wafer-scale MoS₂ and WS₂ single-layer films. Taking advantage of the high-vapor pressure of such precursors, they are placed in bubblers *outside* the growth chamber, thus providing two main improvements: *i.* The precursor delivery to the growth area can be controlled by the carrier gas flow. *ii.* The growth of complex heterostructures can be achieved by changing the precursor flow *during* the growth.²⁰ This means that *in-situ* doping, alloying and heterostructure formation schemes could, in principle, be implemented as well in a controlled manner. However, the use of these volatile precursors was found to have some significant drawbacks. First, in these pioneering works, the growth rate was very slow, a continuous single layer TMDC required about ~26 hrs growth time. Second, the domain size achieved was significantly smaller (usually from few 10s to 100s of nanometers)¹⁵ than the one obtained using the metal – oxide precursors (~100 microns).^{6,8-10}

On the other hand, the electrical and optical quality of most of the CVD-derived 2D TMDCs semiconductors, have often shown to be poorer compared to that of mechanically exfoliated layers from 3D crystals.²¹ Although several chemical treatment methods were developed to restore the intrinsic properties of 2D materials,²²⁻²⁴ implementing such chemical passivation during large-scale processing of 2D semiconductors is challenging. Therefore, despite the extensive research and advance, a reproducible and large-scale growth methodology to produce atomic-layers with high crystal quality is still needed.

In order to improve the CVD (MOCVD)-derived TMDC crystallinity and thus its electrical and optical properties, we refer to three main approaches. The first method relies on the nucleation density reduction/control to obtain larger domains. This was achieved using halide salts (NaCl, KI, etc)^{25,26} and the so called, “seed-promoters”.⁷ In these reports, the domain size was significantly increased to dimensions comparable with those obtained by the metal-oxide approach. However, these seed-suppressing compounds are placed *inside* the growth chamber as well, and thus, some of the inhomogeneities arising from the

distance dependence of the diffusion to/on the growth substrate are relevant here as well. Furthermore, some of these compounds were found to have detrimental effects on the electrical properties of as grown TMDCs.^{27,28} Hence, these approaches may not be suitable for large-scale applications. The second path to improve crystallinity is by the seeded-growth approach, in which well-defined metal (or other) seeds catalyze the nucleation and growth.^{8,29} However, some of the seed material may affect in diverse ways the growth and the resulting optical properties of the grown material.⁸ In addition, implementing this methodology in MOCVD might be difficult due to the very high nucleation density, inhibiting the selective nucleation at the seed. The third approach to improve the crystallinity of the film is to achieve epitaxial growth, usually referred as van der Waals epitaxy in layered materials.³⁰ The basic idea is that the domain size and nucleation density are not as important since the growing domains are well aligned, forming a highly crystalline (possibly single-crystal) film by the coalescence of isolated domains. This was reported in some TMDCs grown on sapphire,^{3,26} GaN³¹ and also on other 2D materials such as graphene and different TMDCs.³²⁻³⁵ Epitaxial growth is however, relatively hard to achieve and the conditions underlying it are not well understood. Another problem in the growth of such atomic films is that, due to the complexity of the precursor flux delivery and the large-number of chemical reactions involved, it is difficult to model and understand the kinetic processes. Obviously, the different chemistries arising from the various precursor types (metal-organics, -chlorides and -oxides) have a significant impact on the nucleation and growth of the TMDC films. This variation in kinetics strongly impacts growth parameters, such as the domain sizes (100s of microns for the metal oxide-based CVD and ~100s of nms for MOCVD). Depending on precursor type, many complex processes may occur simultaneously, such that chemical reaction rates change during the growth due to local concentration variations, possible surface modification of the substrate, domains and domain-edges. All these will dictate eventually the growth type, lateral (2D) versus vertical (3D), and the maximum domain size achievable.

Here we present a “Growth-Etch-MOCVD” (GE-MOCVD) approach to improve the crystallinity of single-layer WS₂ (and WSe₂) layers. The original high-density nucleation is suppressed by the pulsed-delivery of the metal and chalcogen precursors in a constant flow of very low amounts of reactive species (H₂O) in between the growth-cycles. Thus,

carbon contaminants as well as part of the TMDC nuclei are etched and/or re-evaporated, leading to the formation of larger domains with improved crystallinity. We can show an increment of more than four orders of magnitude in the domain size, from few nms to more than 15 microns. The growth evolution of atomic-layers is studied as a function of the H₂O vapor flow, gas composition and cycle number and type. The crystallinity of the GE-MOCVD grown TMDCs is compared to that produced by the standard MOCVD growth processes using Raman and photoluminescence (PL) spectroscopy, as well as high-resolution transmission electron microscope (HRTEM) studies. Furthermore, transient PL measurements show a long fluorescence lifetime, comparable to the emission lifetimes measured from high-quality exfoliated flakes, proving the extraordinary optical quality of the WS₂ films obtained by the GE-MOCVD approach. This methodology could be implemented in the MOCVD growth of many other 2D materials to improve their crystal quality, as required in nanoelectronics and optoelectronics.

Results and Discussion

Figures 1 (a)-(c) show the results for the standard MOCVD growth of WS₂ films, using W(CO)₆ and Di-tert-butyl sulfide (DTBS) as the metal and chalcogen precursors, respectively. Here by “standard” MOCVD we refer to a process in which there is a continuous flow of the precursors and no water vapor is added. The schematic illustration of the customized MOCVD system is depicted in Figure S1. Figures 1(a)-(c) and S2 show typical results of such standard MOCVD growth type. Continuous layers of WS₂ were readily grown and transferred to arbitrary substrates, see experimental section and SI for details. Figure 1(a) shows an optical micrograph of a continuous layer grown on SiO₂(280nm)/Si substrate, which appears non-homogeneous, presumably with ad-layers (darker regions). Raman spectroscopy of such samples exhibits the characteristic WS₂ modes 2LA(M), $E'_{2g}(I)$ and $A_{1g}(I)$ modes, Figure S2(a). Very often, amorphous carbon (a-C) is detected in addition to the WS₂ peaks, as also seen in Figures 1(f) and S2(a), most probably, carbon contamination from the metal-organic precursors. This is one of the disadvantages of using such precursors in CVD.¹¹ Important to note, even at very low powers, the Raman spectroscopy characterization damaged the films, as shown in Figures

S2 (b)-(c), suggesting poor crystal quality. Figure 1(b) shows a low-magnification TEM image of WS₂ transferred to a holey carbon TEM grid. Figure 1(c) displays an HRTEM image of the suspended layer region, in which the lattice of a nanocrystalline (few 10s of nms domain size, yellow dashed lines) film is observed. The FFT of the image in (c), inset, clearly shows a polycrystalline pattern, supporting the nanocrystalline nature of the WS₂ film. This agrees well with reports on MOCVD grown TMDC layers, where domain sizes of up to ~200 nm were observed.^{15-17,36} Larger domains in MOCVD processes were only obtained when adding metal halides to the system.^{15,26} Such unwanted carbon deposition

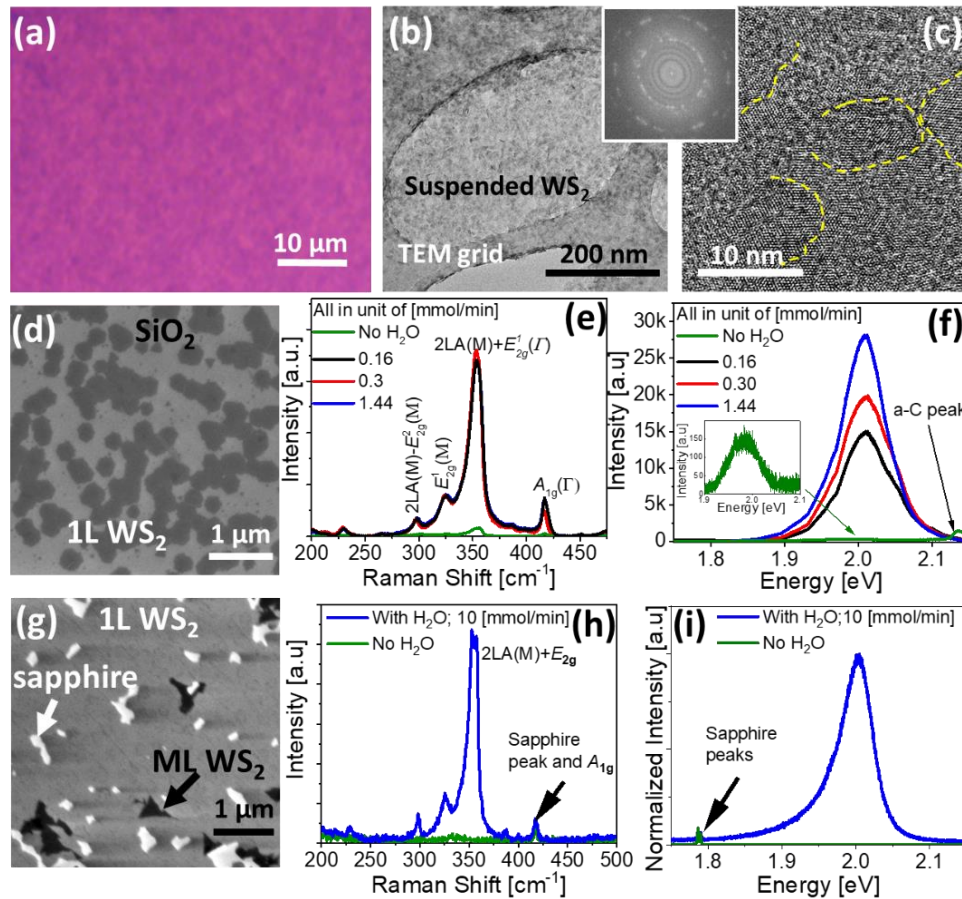


Figure 1: MOCVD growth of WS₂ atomic-layers grown with and without H₂O vapor. (a) – (c) Results obtained for a “standard growth” with no water vapor. Typical optical micrograph (a), low and high resolution TEM micrographs, (b) and (c), of continuous WS₂ atomic-layers grown on SiO₂/Si substrate. The yellow dotted lines in (c) denote the nanocrystalline domains of the continuous film. The inset shows the FFT image recorded from the lattice image shown in (c). (d)-(f) Water-vapor assisted MOCVD growth of WS₂ layers on SiO₂/Si substrate. Typical SEM micrograph (d), comparison of Raman (e), and PL (f) spectra recorded from the samples grown under various concentrations of H₂O. (g)-(i) The same for an H₂O-assisted MOCVD growth on *c*-plane sapphire.

have many detrimental effects, such as serving as nucleation centers, thus increasing the nucleation density (and reducing the domain size), and general contamination of the growth substrate, surface and edges of the domains. In order to diminish this undesirable effect, low amounts of controlled water vapor (~300 ppm) were introduced into the growth chamber. This was achieved by adding N₂ gas from a relatively low purity source (99,99%) and a known humidity (and impurity in general) level. The amount of water in the N₂ gas was measured using a residual gas analyzer (RGA, Figure S3) prior to the growth, see the SI for further details. The addition of water vapor was reported in the past to affect the morphology of the grown domains as well as their crystal quality.^{37,38} In our case, it had an immediate and significant effect as shown in Figures 1(d)-(i). Figure 1(d) shows a SEM image of WS₂ growth on SiO₂/Si with the addition of 0.16 mmol/min of water. Analysis of the different Raman modes demonstrate the films are mostly monolayer in nature. The intensity ratio $I(2LA(M)) / I(A_{1g})$ is found to be ~3.3, confirming the 1L WS₂ nature (Figure S4).³⁹ The PL emission is centered around ~2.0 eV. The Raman and PL spectroscopy of WS₂ domains resulting from the growth under different water vapor concentration in the flow are shown in Figures 1(e) and 1(f), respectively. In both cases, the peak intensity clearly grows with the increased H₂O flow.

Similar results were obtained on sapphire; Figure 1(g) shows the SEM image, highlighting the single-layer (1L), multi-layer (ML) and uncovered sapphire areas. The Raman (Figure 1(h)) and PL (Figure 1(i)) spectra of such samples exhibit higher intensities when the H₂O was added to the growth. The characteristic Raman signature of amorphous carbon detected in the water-free samples disappeared upon the addition of H₂O to the growth process, Figures 1(f) and S2(a). The lack of detectable a-C and the significant increase in the Raman and PL intensities, are a clear indication for the improved crystallinity and purity of the layers. Such an effect can be explained by the reaction of H₂O with the a-C deposited on the sample and its re-evaporation, cleaning both the growth substrate uncovered areas and the domains. Similar results were obtained for WSe₂ atomic-layers (Figure S5(a)-(f)), thus suggesting its generality for the MOCVD growth of TMDs. However, such growth methodology did not change significantly the size of the domains, suggesting there is a limit to the film improvement with the water vapor addition approach. As mentioned above, based on the results summarized in Figures 1(a)-(c) and S2 , as well

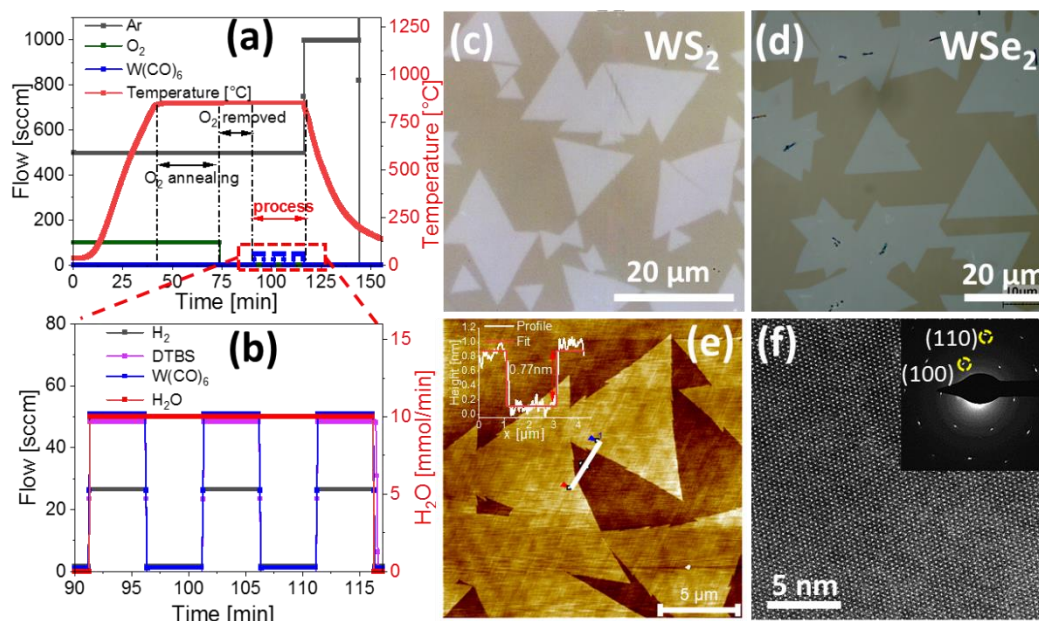


Figure 2: Growth-Etch MOCVD Approach. (a), (b) Flow vs. time charts for the GE-MOCVD growth. (c)-(f) The obtained high-quality atomic-layers; Typical optical micrographs of WS₂ and WSe₂ (c) and (d), respectively. Topography map (e), with the corresponding height profile along the white line. (f) Atomic-resolution HAADF STEM micrograph of a WS₂ single crystalline domain. The SAED pattern recorded from a single crystalline WS₂ domain is shown in the inset in (f), see SI for details.

as previous reports,^{3,15-17,27,36} there is a high nucleation density when using metal-organic precursors. The decomposition temperature of the metal-carbonyls and the carbon contamination could be the cause for this behavior. Therefore, there is a need to partially suppress the nucleation centers in order to allow the domains to expand and grow over larger areas. To achieve this goal, and based on the encouraging growth results with a low concentration of water vapor, a pulsed-growth approach was implemented. In this scheme, the metal and chalcogen precursors were supplied to the system in *pulses* (the “growth” step), while the Ar and water vapor were flown continuously (the “etch” step).

Figure 2 shows the results obtained by the GE-MOCVD approach, in which the gas flow chart as a function of time is depicted in (a)-(b). The precursor pulses and the continuous supply of H₂O are shown in Figure 2(b). The typical optical micrographs of WS₂ and WSe₂, Figures 2 (c) - (d), show a significant increase in the domain size. The AFM topography map of the pristine WS₂ atomic layers shows the monolayer domains of thickness ~ 0.77nm, Figure 2(e). The atomic-resolution HAADF STEM micrographs along with SAED data, inset, show the high crystallinity of the domains (Figures 2(f), S6(a)-(c)). The

microscopy characterization demonstrates the significant improvement in the WS₂ crystal quality grown by the GE-MOCVD approach. As discussed above, the water vapor reacts with the solid carbon contaminants to produce CO gas (and maybe CO₂), causing their re-evaporation and therefore cleaning the substrate and domains. The main sources for the carbon contamination are the W(CO)₆ and the DTBS,^{11,36} therefore, addition of water vapor to a standard-MOCVD growth alone has a limited capability to eliminate such contaminants. This is due to the fact that the precursors are supplied continuously, and hence, the a-C is deposited throughout the growth process. In contrast, in a pulsed-growth method, in which the precursors (W(CO)₆ and DTBS) are supplied in cycles, but the water vapor (and carrier gases) continuously, allows for a successful re-evaporation of the amorphous carbon, thus cleaning the substrate and domains, during the precursor-free pulse, before the growth is continued, significantly improving the domain size and crystal quality.

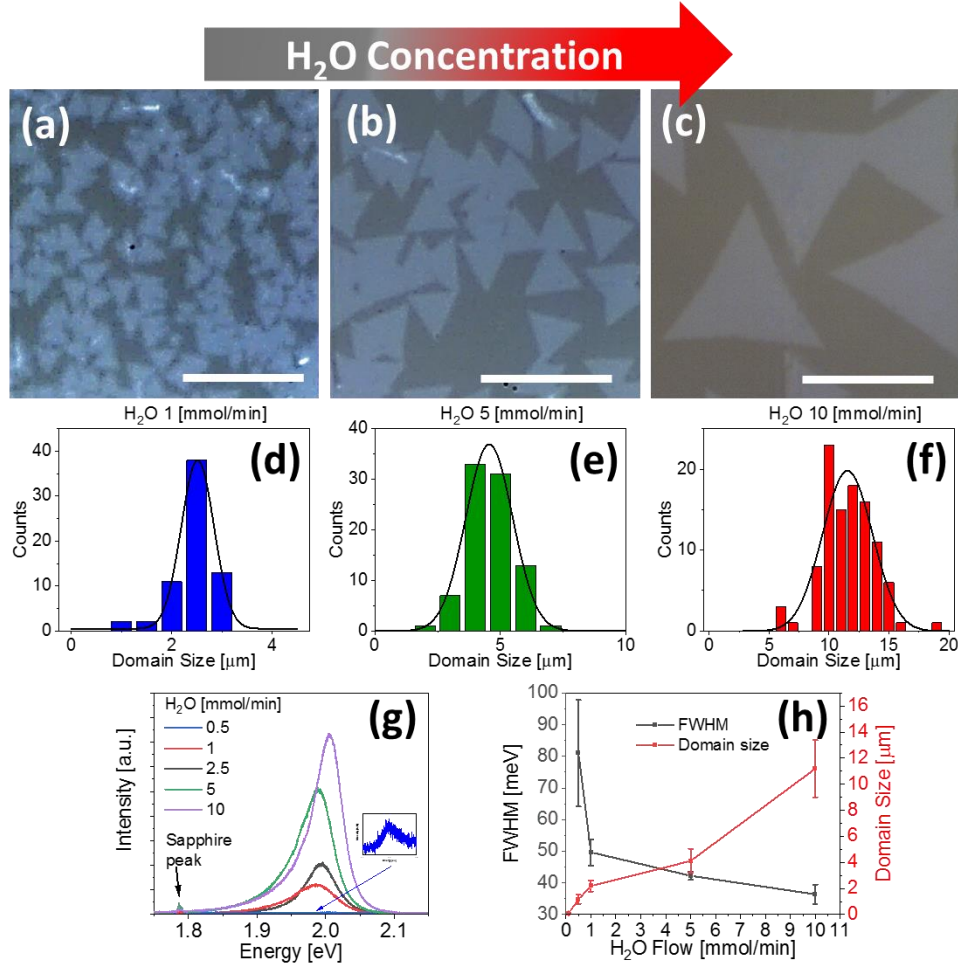


Figure 3: The effect of H₂O concentration in the GE-MOCVD growth. (a)-(c) Typical optical micrographs of WS₂ atomic-layers grown under increased concentration of H₂O; 1, 5, 10 mmol/min. The scale bar is 10 μm. (d)-(f) The corresponding domain size distributions. (g) The comparison of the PL spectra recorded from WS₂ domains grown under different concentrations of H₂O. (h) PL FWHM and domain size as a function of the H₂O concentration, showing a clear domain size evolution with the increased H₂O vapor flow rates.

The effect of the H₂O concentration on the growth is summarized in Figure 3. Figures 3 (a)-(c) show optical images depicting the domain size evolution as a function of H₂O flow, from ~0.1 to 10 mmol/min. The respective domain size distribution is shown in Figures 3 (d)-(f). The PL emission from such samples is plotted in Figure 3(g), in which it is evident that the PL emission intensity increases and full width half-maximum (FWHM) decreases with increased H₂O flow, Figure 3(h), while the domain size increases by more than two

orders of magnitude, from $\sim 0.09 \pm 0.04 \mu\text{m}$ to $11.5 \pm 2.1 \mu\text{m}$, Figure 3(h). The gradual PL emission enhancement, together with the visible increase in the domain size (h), are a clear indication the optical quality and crystallinity are dramatically improved.

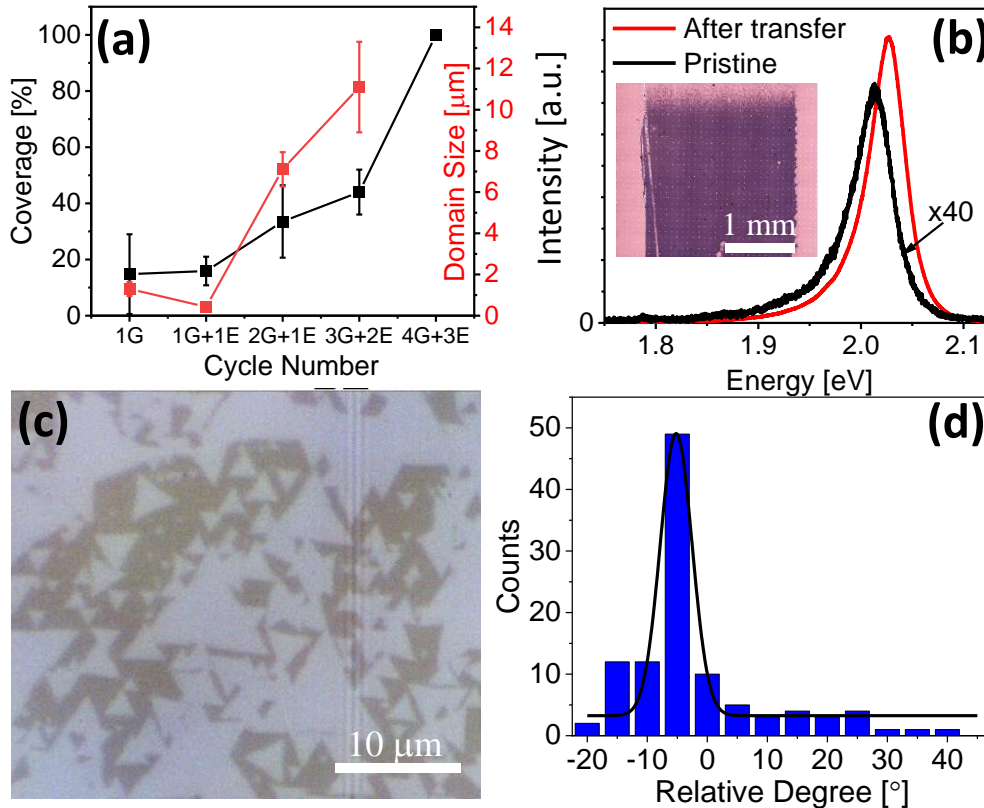


Figure 4: The effect of the cycle # and type on the growth. (a) Area coverage and domain size as a function of cycle # and type. (b) The comparison of PL spectra recorded from WS₂ atomic-layers before and after transfer on to a SiO₂/Si substrate. Inset shows typical optical micrograph after transfer. (c) Optical microscope image of WS₂ domains obtained by a modified 3G+2E cycle, in which the H₂ flow was increase to 50 sccm (from 25) in the last cycle. (d) Angle distribution analysis of pristine domains on *c*-plane sapphire, from (c), showing an improved orientation control.

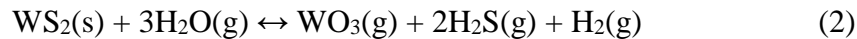
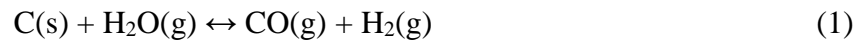
The coverage and domain size change with the type and number of cycles is analyzed and presented in Figure 4. Here the #G and #E refers to the number of cycles in which the precursors (W(CO)₆ and DTBS, #G, “growth step”) and the N₂ (#E - with H₂O, “etch step”) were supplied, see the SI for details. The coverage and the domain size of the WS₂ atomic-layers as a function of the cycle number and type are plotted in Figure 4(a). Both parameters can be controlled via the cycle design in order to achieve a maximum domain size of $\sim 25 \mu\text{m}$ and coverage (100%). Figure 4 (b) shows the PL obtained from a full layer of WS₂

sample grown with a 4G+3E pulse type before (black) and after transferred from sapphire to a SiO₂(280nm)/Si substrate (red), the inset shows the transferred film. Figure 4 (c) shows the optical micrograph of the WS₂ domains obtained in a modified 3G+2E cycle, in which the H₂ flow was doubled (from 25 sccm), in the last pulse. It can be shown that not only the domain size was significantly increased from sub-micron (1G cycle) to more than 10 microns (3G+2E cycle), but also their relative orientation with the substrate is more uniform, plotted in Figure 4 (d). Such result might be an indication of an improved substrate-layer interaction (for example by an H₂-based enhanced surface cleaning of contaminants). Another option could be the selective etching of misoriented domains which are presumably less stable than the epi-grown layers. Further experimental research and theoretical calculations are needed to clarify this important task.

In any vapor-phase growth methods, the carrier gas, in special, the H₂ plays an important role in the growth and by its reaction with residual oxygen and moisture present in such systems. In order to understand the hydrogen role on the TMDC formation, the growth evolution under different flowrates of H₂ is studied. The hydrogen effect on the growth with 1 cycle (1G) is summarized in Figure S7. The nucleation density and domain size as a function of the H₂ flow is plotted in Figure S7(e). A higher H₂ flow, 75 sccm, leads to very high nucleation densities and thus, smaller domain size. The nucleation density is reduced by around three orders of magnitude, with the H₂ flow below 50 sccm. On the other hand, an H₂-free three-cycle growth, Figure S8, leads to very low nucleation density and small dendritic domains. This could be due to an excess of H₂O-based etching of the WS₂ domains, suggesting that some H₂ is necessary to react with the O₂ species present in the system and prevent and slow down the almost complete WS₂ re-evaporation.

Here, we aim to explain the growth mechanism and the results described in the previous sections. The introduction of small amounts of H₂O during the growth and the pulsed delivery of the growth precursors have two main effects; First, it eliminates or diminishes dramatically, the amount of carbon impurity in the films and on the growth substrate, leading to purer and higher quality WS₂ films. Since the presence of amorphous carbon on the substrate may act as a nucleation center, its elimination alone leads to smaller nucleation densities and thus, larger domains. Second, H₂O was shown to etch and re-

evaporate TMDCs,^{37,38,40} therefore, small amounts of water vapor present in the system, react with some of the small/defective WS₂ nuclei/domains causing their re-evaporation, reducing by that the nucleation density as well. Thus, the most relevant reactions taking place during the “etch-step” in which the substrate, and the grown domains, are exposed to water vapor, but not to metal and chalcogen precursors, are the following:^{40,41}



These reactions lead to the re-evaporation of carbon contaminants, (1), and small or defective WS₂ domains, (2). Such reactions cause the *local* concentration of H₂ on the surface to increase. Hence, increasing the H₂ flow, Figure S7, causes an immediate increase in the H₂ concentration in the gas, and therefore, on the substrate as well. This could cause the reactions above to be slowed down and eventually reversed, depending on the surface concentration of H₂. A schematic summarizing the growth processes in a standard- and GE-MOCVD is shown in Figure 5. The top panel represents the “standard”-MOCVD growth in which high nucleation density (thus small domain size) and a-C contaminants are often obtained. The bottom panel in Figure 5 depicts the growth mechanism in the GE-MOCVD approach. The “growth” cycle is followed by an “etch” pulse, where the metal

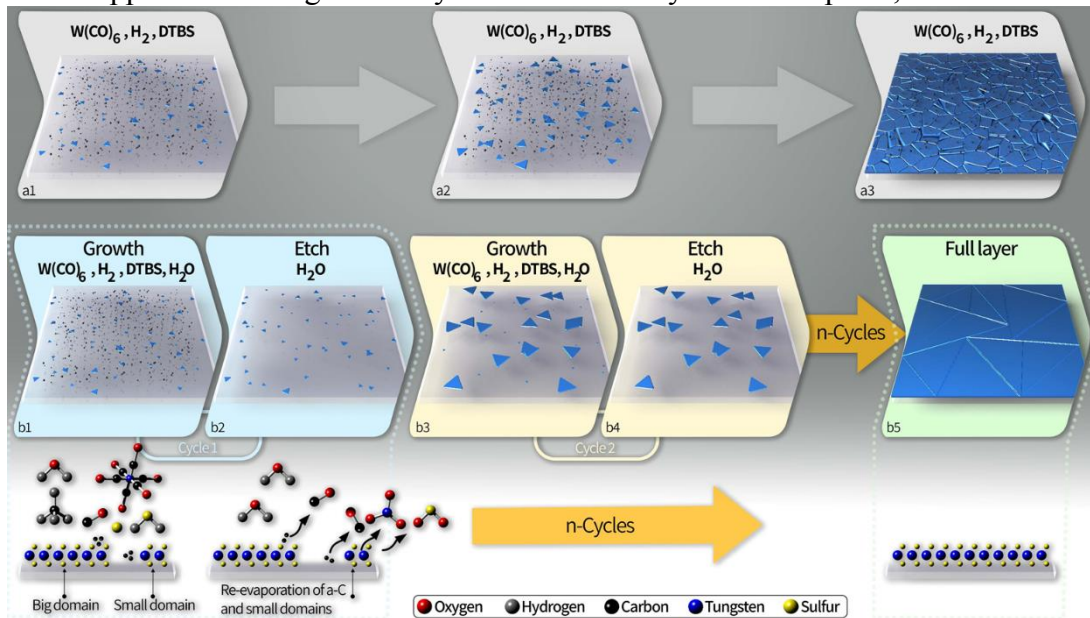


Figure 5: Schematic model of the growth mechanism in a “standard” MOCVD (top) and GE-MOCVD methodologies (bottom).

and chalcogen precursors flow is stopped. This causes the H₂O species to react with the a-C contaminants and small/defective WS₂ (WSe₂) domains, causing their re-evaporation. Therefore, leading to the growth of high-quality TMDC layers.

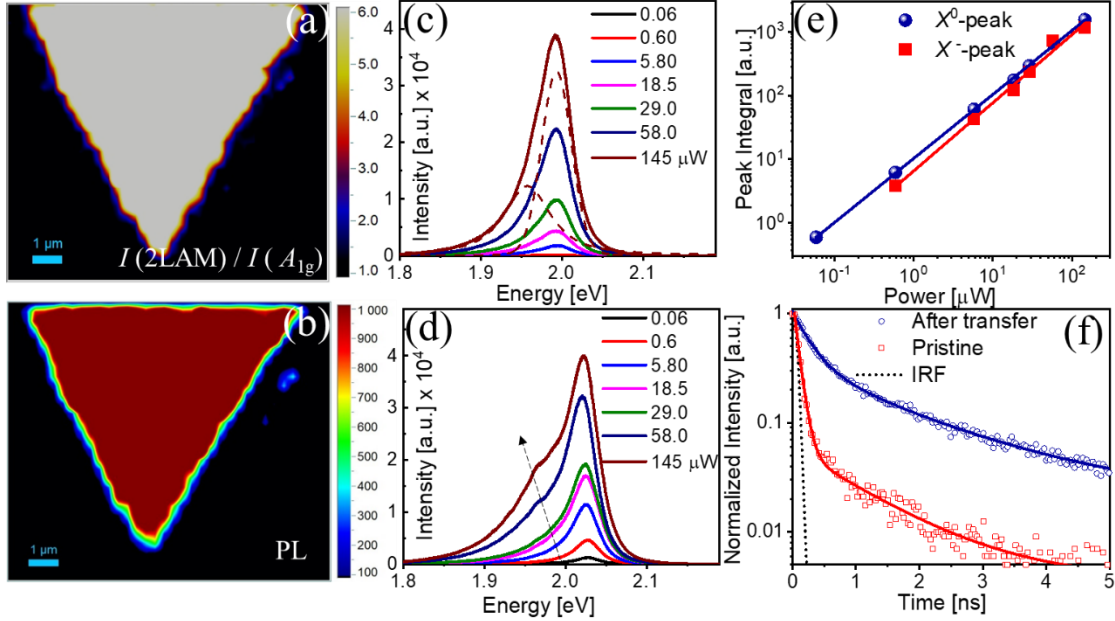


Figure 6: The spectroscopic maps of Raman intensity ratio of 2LAM and A_{1g} modes (a), and PL intensity (b) of single crystalline WS₂ domain, showing uniform monolayer characteristics. Steady-state power dependent PL spectra of (c) pristine and (d) transferred samples of monolayer WS₂ domains. The dashed lines in (c) are the fitted curves corresponding to the highest excitation power spectrum. The dotted arrow in (d) shows the redshift of the low energy peak as a function of excitation power. (e) The PL peak intensities of neutral- A exciton (X^0) and trion (X^-) emissions from pristine domains as a function of excitation power. The solid lines are power law fits of PL intensity. (f) TRPL decay trace measured for a pristine and transferred single crystalline WS₂ domains. The solid lines are exponential decay fits of TRPL curves, and the IRF is plotted in a black dotted line.

Figure S9 shows single crystalline pristine (Figure S9(a)) and transferred (Figure S9(b)) WS₂ domains grown by the GE-MOCVD technique, in addition to the large area continuous atomic layers (Figure S9(c)). The uniform monolayer characteristics of single crystalline WS₂ domain are verified by Raman and PL spectroscopic imaging. Figure S10 (a) shows the optical micrograph of isolated WS₂ domains that were used for such spectroscopic imaging. The Raman map (Figure 6(a)) generated by the intensity ratio of the 2LAM (Figure S10(b)) and A_{1g} (Figure S10(c)) phonon modes shows that the intensity ratio ($I(2LAM) / I(A_{1g})$) is greater than 4, all over the domain, which is a characteristic

nature of the single layer WS₂.³⁹ In addition, the homogeneous optical quality of the single crystalline WS₂ domain is evident from the uniform PL emission associated with the A-excitons, as seen in PL intensity (Figure 6(b)) and PL position (Figure S10(d)) maps.

The optical quality of pristine and transferred WS₂ domains are further studied by conducting steady-state power dependent PL and time resolved PL (TRPL) measurements on single crystalline WS₂ domains. The PL spectra as a function of excitation power recorded from pristine (Figure 6(c)) and transferred (Figure 6(d)) are shown. The spectra recorded from a pristine WS₂ single crystalline domain show an emission around 2.0 eV (Figure 6(c)). The intensity of the PL emission increases as a function of increased excitation power without any appreciable shift in the peak position, indicating no heating effect on the sample due to excitation powers that were used for the measurement. A slight asymmetric broadening on the low energy side of the peak is also seen as the excitation power increases. The strong luminescence around 2.0 eV, can be deconvolved into two peaks. The peak centered at ~1.99 eV is identified as the neutral A-exciton (X^0) emission and the low energy peak around 1.96 eV is attributed to electron-bound exciton (negative trion; X^-) emission.⁸ The neutral exciton emission is stronger than the trion emission at all incident excitation powers. The power (P) dependent PL integrated intensities (I) of both emission peaks are plotted in log-log plot (Figure 6(e)) and fitted with power law, $I = P^b$, where, b is the slope. Both the X^0 ($b = 0.99$) and X^- ($b = 1.06$) emissions show linear behaviour, confirming that there is no trap-assisted recombination through mid-gap states..²³

The transferred WS₂ single crystalline domain PL spectra shows an emission around 2.02 eV at low excitation powers (Figure 6(d)). The intensity of the PL emission increases as a function of increased excitation power without any appreciable shift in the peak center. However, the broadening and intensity of the low energy tail is also enhanced with increased excitation power and evolved into a clear peak centered at ~1.95 eV. Deconvoluted PL spectra presented in Figure S11(b) show that the neutral A-exciton (X^0) emission peak is centered at 2.02 eV and is blue shifted (30 meV) as compared to that of the pristine sample, possibly due to strain relaxation following the transfer from the growth substrate.²² Notably, no appreciable shift of X^0 emission is observed with increased

excitation power. However, the low energy trion emission (X^-) peak has red shifted (Figures 6(d), S11(a), and S11(b)) from 2.0 to 1.97 eV with increased excitation power, indicating the emission is caused by electron-bound exciton (trion) recombination. The trion nature of the low energy peak ~ 1.97 eV is further confirmed by excitation dependent ratio of PL intensity of neutral exciton (X^0) to electron-bound exciton (X^-) emissions (Figure S11(c)). The ratio is increased with excitation power for both pristine and transferred samples. At low powers, both samples showed almost similar values of exciton to trion ratio. However, at high powers the transferred sample showed twice the ratio (X^-/X^0) as compared to that of pristine sample, indicating more free charge carriers bounded with excitons. The relative PL quantum efficiency (PLQE), which is the ratio of emitted PL to incident excitation power, is also an indicative of the optical quality of the samples under comparison. At the lowest excitation intensity, the PLQE is almost two orders higher for transferred WS_2 domains as compared to that of pristine domains (Figure S11(d)), plausibly due to the relaxation of substrate induced strain effects on the WS_2 domains during the growth.²² As the excitation power increases, the PLQE decreased for transferred samples and approached values similar to those of pristine domains at the highest excitation power. The reduction in PLQE at higher powers might be due to the larger trion formation rate by the generation of free charge carriers and the intrinsically low PLQE of trions.²⁴

The high optical quality of the single crystalline WS_2 domains grown by GE-MOCVD technique is further confirmed by studying the exciton dynamics using TRPL. Figure 6(f) shows the TRPL spectra recorded from single crystalline WS_2 domains of pristine and transferred samples, at a pump fluence of ~ 5 $nJ \cdot cm^{-2}$. The normalized TRPL signal of pristine domains is best fitted with biexponential decay having a fast decay time constant (τ_1) of ~ 85 ps and a slow decay time constant (τ_2) of ~ 1.15 ns. TRPL of the transferred WS_2 domains showed fitted by a biexponential decay gave a fast decay time (τ_1) of ~ 270 ps and a slow decay time constants, $\tau_2 \sim 1.47$ ns. We note that for the transferred WS_2 an additional long lived lifetime component (few nsec) was observed but its magnitude was small and for the sake of clarity will not be discussed here further. The fast decay component (τ_1) is attributed to the band edge emission typically shown in TMDCs to be suppressed by the onset of nonradioactive recombination through mid-gap

states, so called trap assisted recombination mechanism. The slow decay time (τ_2) is assigned to radiative recombination from the trion state.⁴² The τ_1 for the transferred WS₂ domains shows 3 times longer as compared to that of pristine domains, indicating the formation of fewer mid-gap states, therefore consistent with higher PLQE as measured in steady-state PL measurements (Figure 11 S(d)) and with the presence of a longer-lived emission component. Interestingly, while the TRPL of the pristine sample show a negligible trion (τ_2) weight component, the trion weight component of the transferred sample is increased by $\times 7.5$, in agreement with the CW measurements (Figure S11(c)). (The τ_1 (~ 85 ps) for pristine WS₂ domains also shows comparable values as that of exfoliated samples ($\tau_1 \sim 64$ ps).²⁴ The highest lifetime of fast decay (τ_1) component measured for the transferred WS₂ domains grown by the GE-MOCVD is found to be ~ 308 ps ($\tau_2 \sim 1.6$ ns) at ~ 0.8 nJ·cm⁻²(Figure S11 S(e)), which is more than 4 times higher than that of as-exfoliated WS₂. The τ_1 and τ_2 values are also comparable to that of the chemical treated exfoliated WS₂ monolayers.²⁴ Such a significant slowing down of nonradiative recombination, highlighting the presence of significantly fewer defect states further confirm the high optical quality of the WS₂ atomic layers grown by the GE-MOCVD technique.

Conclusions

In summary, a novel Growth-Etch MOCVD is developed for the synthesis of ultra-high optical quality WS₂ (and WSe₂) atomic layers. The carbon contamination often present when using metal-organic and the organo-sulfide (and selenide) precursors in standard MOCVD is eliminated via a sequential growth and etch process in which the precursors are delivered to the system in pulses and the continuous flow of low amounts of water vapor. As a result, the ultra-high nucleation density usually obtained in standard MOCVD is highly suppressed by the re-evaporation of the carbon contaminants, and small and defective TMDC nucleus. Therefore, this methodology leads to improved crystallinity and lower contaminants. By understanding the growth evolution in the developed methodology, high crystalline quality TMDCs were achieved with large growth rate. The Raman, steady-

state and time-resolved PL spectroscopy studies established the high crystal and optical quality of the atomic layers grown by the GE-MOCVD. The results obtained here clearly prove that these films have among the highest optical quality for a CVD (or MOCVD)-derived TMDC, comparable to the ones obtained from mechanical exfoliation of a high quality 3D crystal. Hence, the GE-MOCVD method has the potential to address the more acute deficiencies in MOCVD growth of TMDCs, such as the a-C contamination, low growth rate and poor crystallinity. This procedure could be implemented for the synthesis of many other 2D materials and as a proof of concept, the results on WSe₂ showed here. The large-scale growth of high-quality atomic-films is a prerequisite for their integration into a wide range of applications. The work presented here therefore, is a significant step forward for this to happen.

Acknowledgements

The authors gratefully acknowledge the very generous support from the Israel Science Foundation, projects # 2171/17 (A.C. and P.K.M.), 2549/17 (A.P.) and 1784/15 (A.I.).

Experimental

MOCVD and GE-MOCVD Growth

The synthesis of WS₂ was carried out using a hot wall 3 inch customized MOCVD furnace (CVD equipment corporation, model Easy Tube 2000), equipped with 4 separate bubbler for precursors. In one bubbler, Di-tert-butyl sulfide (DTBS, sigma Aldrich, 97%) was loaded inside a glove box under inert gas and the second bubbler was loaded with W(CO)₆ (Strem chemical, 99.9%) in the same glove box. The choice of other source of sulfur was H₂S. For this, we used a scrubber's system to deal with the residual gas. The background and carrier gas used were argon (99.9999%) and hydrogen (99.999%). The substrates, SiO₂ and *c*-plane sapphire (annealed at 1050 °C for 10hrs) were cleaned using acetone and IPA each for 10 minutes in an ultrasonicator and were dried using a nitrogen gun. Prior to the growth, the furnace was evacuated to a pressure down to 15mTorr for 15 minutes to remove

any unwanted moisture/oxygen species. Thereafter, the furnace was ramped to 850 °C at a heating rate of 20 °C/min for 30 minutes under 50 torr with 100sccm of oxygen to remove any possibilities of carbon contamination. Then the oxygen flow was stopped and the system was maintained at the same (850 °C) temperature for another 25 minutes. All the required precursors were then released for the growth. We followed a growth and etch technique in our process cycle as schematically shown in Figures 2 (a)-(b). The process cycle was mainly a combination of two main steps with a period of 5 minutes. In the first step, all the precursors (H₂, DTBS, W(CO)₆, H₂O) were introduced for the growth to take place. In the 2nd step, only H₂O was introduced for the etching process. We repeated this sequence for 3-4 cycle, always terminating with the growth step. The hydrogen and H₂O flow was varied from recipe to recipe. The amount of H₂O introduced was measured by the (residual gas analyzer) RGA technique as described in the SI (Fig. S3). The calculated flow of W(CO)₆ and DTBS was found to be $\sim 3.28 \cdot 10^{-7}$ mol/min and $\sim 3.25 \cdot 10^{-4}$ mol/min respectively, which leads to a sulfur to metal ratio of (S/M) ~ 1000 . The detailed calculations are in the SI.

Transfer of WS₂ to TEM grids, quartz, and SiO₂ substrates

The transfer of WS₂ film from the growth substrate to a new desired substrate was carried out by using a previously reported polystyrene (PS) technique.⁴³ In this process, 450 mg of PS (280000 g/mol) was dissolved in 5 ml of toluene. The PS solution was then spin-coated (60 seconds at 3500 rpm) onto the as-grown WS₂ layer on sapphire to make a thin film of PS. Thereafter, the sample was backed at 90 °C for 30 minutes and then at 120 °C for 10 minutes. The polymer/WS₂ assembly was delaminated by allowing the water to penetrate in between sapphire and the assembly. The floating layer was then fished out of the water to any desired substrate (TEM grid, quartz or SiO₂) and left for drying naturally at room temperature. Another baking process (90 °C for 30 minutes and more 15 minutes at 120 °C) was adopted to ensure no water residuals were left in the interface. In the end, the PS film was dissolved from the assembly by using toluene.

HRTEM and HAADF measurements

High-resolution scanning transmission electron microscopy (HRSTEM) images were recorded in a double aberration-corrected Themis Z microscope (Thermo Fisher Scientific

Electron Microscopy Solutions, Hillsboro, USA) equipped with a high-brightness FEG at an accelerating voltage of 80kV. High-resolution TEM images were collected on the Themis-Z instrument on a Gatan One View CMOS camera (Gatan Inc., Pleasanton, USA) at negative spherical aberration settings ($C_s = -20\mu\text{m}$) with higher order axial aberrations corrected up to 30 mrad.

Atomic force microscopy (AFM)

Topographic characterization was performed using a Nanosurf Core AFM in tapping mode.

Raman and Photoluminescence Spectroscopy

The Raman and PL spectroscopy measurements were conducted using a confocal micro-Raman (PL) spectrometer (Horiba, LabRAM HR Evolution). The as-grown samples were excited using an excitation laser of 532 nm and collected the scattered radiation using x100 objective (0.9 NA). The scattered radiation was analyzed and detected using a grating of 1800 gr.mm^{-1} and, thermoelectrically cooled CCD detector, respectively. The Raman and PL spectral imaging were performed on a software controlled XYZ motorized stage with a step resolution of $\sim 100\text{ nm}$. The laser power, exposure and collection timings were optimized to record the Raman and PL imaging.

Time-resolved photoluminescence (TRPL) Spectroscopy measurements:

TRPL Spectroscopy measurements were performed using a home-built setup. The spectra were collected from the pristine samples on sapphire and the samples transferred on to quartz substrate. A pulsed laser of wavelength 405 nm (EPL-405nm, 55 ps pulse width) was used to excite the samples mounted on an inverted microscope (Zeiss). An oil-immersion objective lens (63 \times ; NA: 1.4) was used to focus the incident laser and collect the PL signals in a confocal configuration and filtered by passing through the 488 nm dichroic mirror and 595 nm long pass filter. Prior to the TRPL, the point of interest was chosen by imaging onto a CCD (Andor, iXon Ultra). PL lifetimes were collected using a single photon avalanche photo diode (SPAD) (ID100, ID Quantique) coupled to a time-correlated single photon counter (TCSPC) module (HydraHarp 400, PicoQuant). The power dependent TRPL measurements were performed by varying the laser power using a set of ND filters and measuring the power by a powermeter (Nova II, Ophir).

References

- 1 Lee, Y.-H. *et al.* Synthesis of Large-Area MoS₂ Atomic Layers with Chemical Vapor Deposition. *Advanced Materials* **24**, 2320-2325, doi:10.1002/adma.201104798 (2012).
- 2 Hod, O., Urbakh, M., Naveh, D., Bar-Sadan, M. & Ismach, A. Flatlands in the Holy Land: The Evolution of Layered Materials Research in Israel. *Advanced Materials* **0**, 1706581, doi:10.1002/adma.201706581 (2018).
- 3 Eichfeld, S. M. *et al.* Highly Scalable, Atomically Thin WSe₂ Grown via Metal-Organic Chemical Vapor Deposition. *Acs Nano* **9**, 2080-2087, doi:10.1021/nn5073286 (2015).
- 4 Yang, P. *et al.* Influence of seeding promoters on the properties of CVD grown monolayer molybdenum disulfide. *Nano Research* **12**, 823-827, doi:10.1007/s12274-019-2294-y (2019).
- 5 Teich, J. *et al.* Light and complex 3D MoS₂/graphene heterostructures as efficient catalysts for the hydrogen evolution reaction. *Nanoscale* **12**, 2715-2725, doi:10.1039/c9nr09564k (2020).
- 6 Liu, Y. *et al.* Mesoscale Imperfections in MoS₂ Atomic Layers Grown by a Vapor Transport Technique. *Nano Letters* **14**, 4682-4686, doi:10.1021/nl501782e (2014).
- 7 Ling, X. *et al.* Role of the Seeding Promoter in MoS₂ Growth by Chemical Vapor Deposition. *Nano Letters* **14**, 464-472, doi:10.1021/nl4033704 (2014).
- 8 Patsha, A., Sheff, V. & Ismach, A. Seeded-growth of WS₂ atomic layers: the effect on chemical and optical properties. *Nanoscale* **11**, 22493-22503, doi:10.1039/c9nr06515f (2019).
- 9 Yun, S. J. *et al.* Synthesis of Centimeter-Scale Monolayer Tungsten Disulfide Film on Gold Foils. *ACS Nano* **9**, 5510-5519, doi:10.1021/acsnano.5b01529 (2015).
- 10 Radovsky, G., Shalev, T. & Ismach, A. Tuning the morphology and chemical composition of MoS₂ nanostructures. *Journal of Materials Science* **54**, 7768-7779, doi:10.1007/s10853-019-03437-4 (2019).
- 11 Jones, A. C. & Hitchman, M. L. *Chemical vapour deposition : precursors, processes and applications*. xv, 582 pages : illustrations, plans ; 26 cm (Royal Society of Chemistry, 2009).
- 12 Yu, H. *et al.* Wafer-Scale Growth and Transfer of Highly-Oriented Monolayer MoS₂ Continuous Films. *ACS Nano* **11**, 12001-12007, doi:10.1021/acsnano.7b03819 (2017).
- 13 Chiu, H. T. & Chuang, S. H. TUNGSTEN NITRIDE THIN-FILMS PREPARED BY MOCVD. *Journal of Materials Research* **8**, 1353-1360, doi:10.1557/jmr.1993.1353 (1993).
- 14 Hofmann, W. K. THIN-FILMS OF MOLYBDENUM AND TUNGSTEN DISULFIDES BY METAL ORGANIC-CHEMICAL VAPOR-DEPOSITION. *Journal of Materials Science* **23**, 3981-3986, doi:10.1007/bf01106824 (1988).
- 15 Kang, K. *et al.* High-mobility three-atom-thick semiconducting films with wafer-scale homogeneity. *Nature* **520**, 656-660, doi:10.1038/nature14417 (2015).
- 16 Kalanyan, B. *et al.* Rapid Wafer-Scale Growth of Polycrystalline 2H-MoS₂ by Pulsed Metal-Organic Chemical Vapor Deposition. *Chemistry of Materials* **29**, 6279-6288, doi:10.1021/acs.chemmater.7b01367 (2017).
- 17 Lee, D. H., Sim, Y., Wang, J. & Kwon, S. Y. Metal-organic chemical vapor deposition of 2D van der Waals materials-The challenges and the extensive future opportunities. *Appl Materials* **8**, doi:10.1063/1.5142601 (2020).

- 18 Cwik, S. *et al.* Direct Growth of MoS₂ and WS₂ Layers by Metal Organic Chemical Vapor
Deposition. *Advanced Materials Interfaces* **5**, doi:10.1002/admi.201800140 (2018).
- 19 Andrzejewski, D. *et al.* Improved luminescence properties of MoS₂ monolayers grown via
MOCVD: role of pretreatment and growth parameters. *Nanotechnology* **29**,
doi:10.1088/1361-6528/aabbb9 (2018).
- 20 Xie, S. E. *et al.* Coherent, atomically thin transition-metal dichalcogenide superlattices
with engineered strain. *Science* **359**, 1131-1135, doi:10.1126/science.aao5360 (2018).
- 21 Choi, W. *et al.* Recent development of two-dimensional transition metal dichalcogenides
and their applications. *Materials Today* **20**, 116-130,
doi:https://doi.org/10.1016/j.mattod.2016.10.002 (2017).
- 22 Amani, M. *et al.* High Luminescence Efficiency in MoS₂ Grown by Chemical Vapor
Deposition. *ACS Nano* **10**, 6535-6541, doi:10.1021/acsnano.6b03443 (2016).
- 23 Amani, M. *et al.* Recombination Kinetics and Effects of Superacid Treatment in Sulfur- and
Selenium-Based Transition Metal Dichalcogenides. *Nano Letters* **16**, 2786-2791,
doi:10.1021/acs.nanolett.6b00536 (2016).
- 24 Tanoh, A. O. A. *et al.* Enhancing Photoluminescence and Mobilities in WS₂ Monolayers
with Oleic Acid Ligands. *Nano Letters* **19**, 6299-6307, doi:10.1021/acs.nanolett.9b02431
(2019).
- 25 Li, S. S. *et al.* Halide-assisted atmospheric pressure growth of large WSe₂ and WS₂
monolayer crystals. *Applied Materials Today* **1**, 60-66, doi:10.1016/j.apmt.2015.09.001
(2015).
- 26 Kim, H., Ovchinnikov, D., Deiana, D., Unuchek, D. & Kis, A. Suppressing Nucleation in
Metal-Organic Chemical Vapor Deposition of MoS₂ Monolayers by Alkali Metal Halides.
Nano Letters **17**, 5056-5063, doi:10.1021/acs.nanolett.7b02311 (2017).
- 27 Zhang, K. H. *et al.* Considerations for Utilizing Sodium Chloride in Epitaxial Molybdenum
Disulfide. *Acs Applied Materials & Interfaces* **10**, 40831-40837,
doi:10.1021/acsmi.8b16374 (2018).
- 28 Utama, M. I. B., Lu, X., Yuan, Y. W. & Xiong, Q. H. Detrimental influence of catalyst seeding
on the device properties of CVD-grown 2D layered materials: A case study on MoSe₂.
Applied Physics Letters **105**, doi:10.1063/1.4904945 (2014).
- 29 Han, G. H. *et al.* Seeded growth of highly crystalline molybdenum disulphide monolayers
at controlled locations. *Nature Communications* **6**, doi:10.1038/ncomms7128 (2015).
- 30 Koma, A. VANDERWAALS EPITAXY - A NEW EPITAXIAL-GROWTH METHOD FOR A HIGHLY
LATTICE-MISMATCHED SYSTEM. *Thin Solid Films* **216**, 72-76, doi:10.1016/0040-
6090(92)90872-9 (1992).
- 31 Zhang, K. H. *et al.* Large scale 2D/3D hybrids based on gallium nitride and transition metal
dichalcogenides. *Nanoscale* **10**, 336-341, doi:10.1039/c7nr07586c (2018).
- 32 Fu, W. *et al.* Room Temperature Commensurate Charge Density Wave on Epitaxially
Grown Bilayer 2H-Tantalum Sulfide on Hexagonal Boron Nitride. *Acs Nano* **14**, 3917-3926,
doi:10.1021/acsnano.0c00303 (2020).
- 33 Liu, X. L. *et al.* Rotationally Commensurate Growth of MoS₂ on Epitaxial Graphene. *Acs
Nano* **10**, 1067-1075, doi:10.1021/acsnano.5b06398 (2016).
- 34 Zhang, X. *et al.* Vertical Heterostructures of Layered Metal Chalcogenides by van der
Waals Epitaxy. *Nano Letters* **14**, 3047-3054, doi:10.1021/nl501000k (2014).
- 35 Mohapatra, P. K., Ranganathan, K., Dezanashvili, L., Houben, L. & Ismach, A. Epitaxial
Growth of In₂Se₃ on Monolayer Transition Metal Dichalcogenide Single Crystals for High
Performance Photodetectors. *Applied Materials Today In Press* (2020).

- 36 Zhang, X. T. *et al.* Influence of Carbon in Metalorganic Chemical Vapor Deposition of Few-Layer WSe₂ Thin Films. *Journal of Electronic Materials* **45**, 6273-6279, doi:10.1007/s11664-016-5033-0 (2016).
- 37 Choi, S. H. *et al.* Water-Assisted Synthesis of Molybdenum Disulfide Film with Single Organic Liquid Precursor. *Scientific Reports* **7**, doi:10.1038/s41598-017-02228-8 (2017).
- 38 Kastl, C. *et al.* The important role of water in growth of monolayer transition metal dichalcogenides. *2d Materials* **4**, doi:10.1088/2053-1583/aa5f4d (2017).
- 39 Berkdemir, A. *et al.* Identification of individual and few layers of WS₂ using Raman Spectroscopy. *Scientific Reports* **3**, 1755, doi:10.1038/srep01755 (2013).
- 40 Cannon, P. & Norton, F. J. Reaction between Molybdenum Disulphide and Water. *Nature* **203**, 750-751, doi:10.1038/203750a0 (1964).
- 41 Millner, T. & Neugebauer, J. Volatility of the Oxides of Tungsten and Molybdenum in the Presence of Water Vapour. *Nature* **163**, 601-602, doi:10.1038/163601b0 (1949).
- 42 Zhang, X. X., You, Y. M., Zhao, S. Y. F. & Heinz, T. F. Experimental Evidence for Dark Excitons in Monolayer WSe₂. *Physical Review Letters* **115**, doi:10.1103/PhysRevLett.115.257403 (2015).
- 43 Gurarlsan, A. *et al.* Surface-Energy-Assisted Perfect Transfer of Centimeter-Scale Monolayer and Few-Layer MoS₂ Films onto Arbitrary Substrates. *ACS Nano* **8**, 11522-11528, doi:10.1021/nn5057673 (2014).